

# Geometric Conditions for Lossless Convexification in Fuel-Optimal Control of Linear Systems with Discrete-Valued Inputs

Felipe Arenas-Uribe, Hasan A. Poonawala, and Jesse B. Hoagg

**Abstract**— Trajectory generation for autonomous systems with discrete-valued actuators is challenging due to the mixed-integer nature of the resulting optimization problems, which are generally intractable for real-time, safety-critical applications. Lossless convexification offers an alternative by reformulating mixed-integer programs as equivalent convex programs that can be solved efficiently with guaranteed convergence. This paper develops a lossless convexification framework for the fuel-optimal control of linear systems with discrete-valued inputs. We extend existing Mayer-form results by showing that, under simple geometric conditions, system normality is preserved when reformulating Lagrange-form problems into Mayer-form. Furthermore, we derive explicit algebraic conditions for normality in systems with cross-polytopic input sets. Leveraging these results and an extreme-point relaxation, we demonstrate that the fuel-optimal control problem admits a lossless convexification, enabling real-time, discrete-valued solutions without resorting to mixed-integer optimization. Numerical results from Monte Carlo simulations confirm that the proposed approach consistently yields discrete-valued control inputs with computation times compatible with real-time implementation.

## I. INTRODUCTION

Discrete-valued inputs are common in autonomous systems, as many actuators operate in an on-off manner or with finitely many magnitude levels. Examples include relays, transistors, and flow-control valves. Direct trajectory-generation methods for such systems are computationally challenging because the discrete actuator behavior introduces mixed-integer constraints into the optimization problem. Mixed-Integer Convex Programs (MICPs) are inherently difficult to solve, lacking general convergence guarantees and exhibiting exponential growth in runtime with the number of decision variables [1]. These computational challenges render MICPs unsuitable for safety-critical, real-time applications such as aerospace guidance and autonomous vehicle control [2].

Recent work has used machine learning to warm-start MICP solvers and thereby accelerate their convergence [3], [4], but these data-driven methods provide no formal guarantees of optimality or convergence. In contrast, theoretical research has focused on directly analyzing optimal control problems (OCPs), which are commonly categorized into three standard forms: the *Mayer form* (terminal cost), *Lagrange form* (running cost), and *Bolza form* (combined running and terminal costs). In particular, lossless convexification has shown that certain MICPs can be reformulated as equivalent convex programs (CPs) without loss of optimality, offering a computationally tractable alternative [5]. A lossless

Felipe Arenas-Uribe, Hasan A. Poonawala, and Jesse B. Hoagg are with the Department of Mechanical and Aerospace Engineering, University of Kentucky, Lexington, KY, USA. (e-mail: felipeaur@uky.edu).

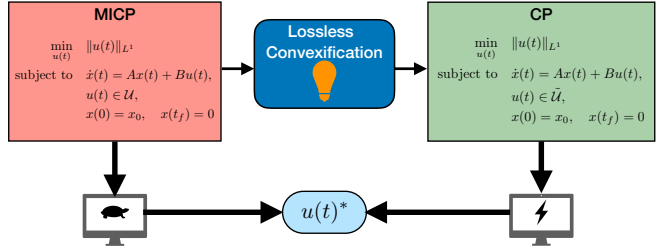


Fig. 1. Lossless convexification enables real-time, fuel-optimal trajectory generation by solving a convex program instead of a Mixed-Integer Convex Program.

convexification method for Mayer-form OCPs with linear time-invariant (LTI) systems and disconnected input sets was introduced in [6], where system normality and an extreme-point relaxation were exploited to achieve an exact convex reformulation. Similarly, [7] exploited strong observability to obtain a lossless convexification of an LTI time-optimal control problem with state constraints.

Despite these advances, existing results are limited to Mayer-form OCPs, and no formal results have been established for Lagrange-form OCPs. It was proposed in [6] that Lagrange-form problems can be reformulated as Mayer-form problems via an epigraph transformation; however, it remains unclear whether system normality is preserved under this transformation. Lagrange-form OCPs include the fuel-optimal control problem, where the  $L^1$ -norm of the control input serves as the cost function since it is proportional to the total control effort [8]. This problem is particularly relevant in spacecraft applications, where maximizing mission lifetime requires minimizing fuel consumption during each maneuver. In practice, continuous quadratic approximations of the  $L^1$ -norm are often used [9], but these yield suboptimal trajectories and can reduce mission longevity. Furthermore, spacecraft typically employ discrete-valued actuators, such as cold-gas thrusters for reaction control systems [10], introducing mixed-integer constraints into the trajectory optimization problem. Notably, the fuel-optimal control problem has also been shown to be equivalent to the maximum hands-off control problem [11], further underscoring the importance of developing a lossless convexification for this class of Lagrange-form OCPs.

In this paper, we extend the theory of Mayer-form MICP relaxations and show that the fuel-optimal control problem for linear systems with discrete-valued inputs can be reformulated as a Mayer-form MICP while preserving system normality, under an assumption on the geometric structure of the input set. Exploiting this structure, we derive a simple algebraic condition that verifies normality directly from the

system matrices. Building on [6], we demonstrate that the resulting Mayer-form MICP can be solved exactly as a convex optimization problem by leveraging system normality and an extreme-point relaxation of the input set. Consequently, the original fuel-optimal control problem with discrete-valued actuators can be solved efficiently using convex optimization (see Fig. 1).

We validate the proposed approach through numerical experiments on a spacecraft rendezvous scenario. The results show that the generated control inputs are inherently discrete-valued and that this discreteness is maintained even under coarser discretization grids. Furthermore, Monte Carlo simulations confirm that the method consistently produces discrete-valued control solutions with computation times compatible with real-time requirements, such as those specified by NASA's SPLICE project [12].

## II. PROBLEM FORMULATION

Let  $\mathbb{N}_{>0}$  be the set of positive natural numbers not including 0. Let  $\mathcal{A} \subset \mathbb{R}^n$  be a set. Then, the convex hull of  $\mathcal{A}$  is  $\text{conv}(\mathcal{A})$ , the extreme points of  $\mathcal{A}$  is  $\text{ex}(\mathcal{A})$ , and the boundary of  $\mathcal{A}$  is  $\text{bd}(\mathcal{A})$ .

### A. Discrete-Valued Control Inputs

The input set  $\mathcal{U}$  is the finite disconnected set defined as

$$\mathcal{U} \triangleq \{0, u_1, u_2, \dots, u_\ell\},$$

where  $u_i \in \mathbb{R}^m$ ,  $i = 1, \dots, \ell$  and  $\ell \in \mathbb{N}_{>0}$ . We make the assumption:

(A1) For every  $u \in \text{ex}(\text{conv}(\mathcal{U}))$ ,  $\|u\|_1 = \max_{v \in \mathcal{U}} \|v\|_1$ .

An admissible discrete set which satisfies this assumption is one in which the actuators are limited by a maximum magnitude  $u_{\max} > 0$ , and the admissible combinations are constrained such that the 1-norm of the input vector does not exceed this bound. This family of sets can be defined as

$$\mathcal{U} \triangleq \{0\} \cup \{\pm u_{\max} e_i\}_{i=1}^m \cup \mathcal{W}, \quad (1)$$

where  $e_i$  denotes the  $i$ -th standard basis vector in  $\mathbb{R}^m$ , and  $\mathcal{W} \subset \{u \in \mathbb{R}^m : \|u\|_1 \leq u_{\max}\}$  is a finite set of additional actuator combinations. This structure is common in systems where multiple actuators share a limited total control authority, such as in multi-thruster spacecraft or multi-rotor vehicles. The technical importance of assumption (A1) will be explained in section V. By focusing on the family of sets which satisfy this assumption, a family of polytopes known as cross-polytopes emerge as we study the geometry of the set  $\text{conv}(\mathcal{U})$ .

**Definition 1.** An  $m$ -dimensional *cross-polytope* is the closed 1-ball of radius  $u_{\max} > 0$

$$\mathcal{C}_m(u_{\max}) \triangleq \{u \in \mathbb{R}^m : \|u\|_1 \leq u_{\max}\}.$$

Equivalently, it is the convex hull of the  $2m$  points  $\{\pm u_{\max} e_i\}_{i=1}^m$ , where  $e_i$  are the standard basis vectors of  $\mathbb{R}^m$ .

**Fact 1.** Consider the set  $\mathcal{U}$ . Then,  $\text{conv}(\mathcal{U}) = \mathcal{C}_m(u_{\max})$ . Moreover, for every  $u \in \text{ex}(\text{conv}(\mathcal{U}))$ , it holds that  $\|u\|_1 = \max_{v \in \mathcal{U}} \|v\|_1$ .

*Proof.* By construction, the set  $\mathcal{U}$  in (1) contains all of the vertices  $\{\pm u_{\max} e_i\}_{i=1}^m$ , where  $e_i$  are the standard basis vectors of  $\mathbb{R}^m$ . The additional points in  $\mathcal{W}$  lie strictly within the 1-ball of radius  $u_{\max}$ , and the origin is also included. Therefore, taking the convex hull of  $\mathcal{U}$  does not introduce any new extreme points. Consequently,  $\text{conv}(\mathcal{U}) = \text{conv}(\{\pm u_{\max} e_i\}_{i=1}^m)$ , which is, by definition, an  $m$ -dimensional cross-polytope of radius  $u_{\max}$ .

Since  $\text{conv}(\mathcal{U})$  is a cross-polytope, its extreme points are exactly the  $2m$  vertices  $\{\pm u_{\max} e_i\}_{i=1}^m$ . Each of these satisfies  $\|u_{\max} e_i\|_1 = u_{\max}$ . Hence, for every  $u \in \text{ex}(\text{conv}(\mathcal{U}))$ ,  $\|u\|_1 = u_{\max} = \max_{v \in \mathcal{U}} \|v\|_1$ , which proves the claim.  $\square$

Fact 1 shows that, by exploiting the geometrical properties of cross-polytopes, we naturally satisfy (A1), thereby proving that this assumption does not restrict the applicability of our results.

### B. Fuel-Optimal Discrete-Valued Control Problem

Consider the linear time-invariant system

$$\dot{x}(t) = Ax(t) + Bu(t), \quad (2)$$

where  $A \in \mathbb{R}^{n \times n}$ ,  $B \in \mathbb{R}^{n \times m}$ ,  $x(t) \in \mathbb{R}^n$  is the state,  $x(0) = x_0 \in \mathbb{R}^n$  is the initial condition, and  $u(t) \in \mathcal{U} \subset \mathbb{R}^m$  is the input. We make the assumption:

(A2) The pair  $(A, B)$  is controllable.

Let  $t_f > 0$  be a fixed final time. Our objective is to find a control  $u(t) \in \mathcal{U}$  on  $[0, t_f]$  that drives the state from  $x_0$  to the origin, while minimizing the  $L^1$ -norm of the control input  $u(t)$ .

### Problem 1. Fuel-Optimal Mixed-Integer Problem

$$\min_{u(t)} \int_0^{t_f} \|u(t)\|_1 dt \quad (3a)$$

$$\text{subject to } \dot{x}(t) = Ax(t) + Bu(t), \quad (3b)$$

$$u(t) \in \mathcal{U}, \quad (3c)$$

$$x(0) = x_0, \quad x(t_f) = 0 \quad (3d)$$

The cost function (3a) is convex but non-differentiable at points where the control input vanishes. As a result, optimization problems involving the  $L^1$ -norm often require subgradient methods or equivalent convex reformulations. Moreover, the discrete-valued nature of the control input introduces integer constraints, making Problem 1 a mixed-integer convex program (MICP). The computational limitations of MICP solvers are particularly restrictive in real-time control applications, where efficiency and convergence guarantees are critical.

## III. NORMALITY AND EXTREME POINT RELAXATIONS

Let  $p(t) \in \mathbb{R}^n$  be the costate vector associated with (2). The Hamiltonian of Problem 1 is defined as

$$H_1(x, u, p) \triangleq \|u\|_1 + p^\top (Ax + Bu) \quad (4)$$

Since  $B$  is continuous and  $\mathcal{U}$  is a fixed compact set, it follows from the Minimum Principle [13, Theorem 6.7.1] that there exists an optimal control  $u^*(t)$  that satisfies the Hamiltonian minimization condition point-wise in time,

$$u^*(t) \in \arg \min_{u \in \mathcal{U}} \left\{ H_1(x(t), u, p(t)) \right\}, \quad (5)$$

for almost every  $t \in [0, t_f]$ .

A difficulty arises if the minimizer of (5) over  $\mathcal{U}$  is not unique, since in that case the Minimum Principle does not determine a single control law. A non-unique minimizer implies that the optimal control law is not well-defined, potentially leading to ambiguous and non-unique system trajectories. To exclude this degeneracy, the notion of normality is defined [13, definition 6.7.4].

**Definition 2.** The system (2) is said to be *normal* with respect to  $\mathcal{U}$  on an interval  $[0, t_f]$  if, for every nonzero vector  $p(0) \in \mathbb{R}^n$  and for almost every  $t \in [0, t_f]$ , the Hamiltonian minimization condition (5) admits a unique solution  $u^*(t) \in \mathcal{U}$ .

The next result provides sufficient conditions for normality of the system based on the geometric properties of the input set  $\mathcal{U}$ , this is motivated by [13, corollary 6.7.15].

**Lemma 1.** Consider the system (2) and the input set  $\mathcal{U}$ , and let  $\tilde{\mathcal{U}} = \text{conv}(\mathcal{U})$ . Then,  $(A, B)$  is normal with respect to  $\tilde{\mathcal{U}}$ .

*Proof.* Suppose for contradiction that  $(A, B)$  is controllable but not normal with respect to  $\tilde{\mathcal{U}}$ . Then, there exists a nonzero costate vector  $p(t) \in \mathbb{R}^n$  satisfying the adjoint equation

$$\dot{p}(t) = -A^\top p(t),$$

such that

$$p(t)^\top Bu = 0 \quad \forall u \in \tilde{\mathcal{U}}, \quad \forall t \in [0, t_f].$$

By the Krein–Milman theorem [14], any compact convex set is the convex hull of its extreme points. Hence, it suffices to check the condition on the finite vertex set  $\text{ex}(\tilde{\mathcal{U}}) \subseteq \mathcal{U}$ , giving

$$p(t)^\top Bu = 0, \quad \forall u \in \text{ex}(\tilde{\mathcal{U}}), \quad \forall t \in [0, t_f].$$

Since  $A$  and  $B$  are constant, the solution of the adjoint equation is

$$p(t) = p_0 e^{-A^\top t}, \quad p_0 = p(0).$$

Evaluating at  $t = 0$  shows that

$$p_0^\top Bu = 0, \quad \forall u \in \text{ex}(\tilde{\mathcal{U}}).$$

Controllability of  $(A, B)$  then implies  $p_0 = 0$ , and hence  $p(t) \equiv 0$ . This contradicts the assumption that a nonzero costate exists. Therefore,  $(A, B)$  is normal with respect to  $\tilde{\mathcal{U}}$ .  $\square$

Additionally, a fundamental implication of normality is formalized in the following lemma [13, Corollary 6.7.7].

**Lemma 2.** Consider the system (2) and the set  $\tilde{\mathcal{U}} = \text{conv}(\mathcal{U})$ . Let the system  $(A, B, \tilde{\mathcal{U}})$  be normal. If  $u(t)$  is

an optimal control, then  $u(t) \in \text{ex}(\tilde{\mathcal{U}})$  for almost every  $t \in [0, t_f]$ .

This result implies that the optimal control  $u$  can only take values from a finite set given by the vertices of  $\tilde{\mathcal{U}}$ , which motivates the extreme point relaxation introduced in [6, Theorem 1].

**Lemma 3.** Consider Problem 1 and let the cost function be a terminal cost function (i.e. Mayer-form OCP). Consider a relaxed input set  $\tilde{\mathcal{U}} \subset \mathbb{R}^m$  and assume  $\tilde{\mathcal{U}}$  satisfies the conditions:

- (C1)  $\tilde{\mathcal{U}}$  is compact and convex.
- (C2)  $\mathcal{U} \subset \tilde{\mathcal{U}}$ .
- (C3)  $\text{ex}(\tilde{\mathcal{U}}) \subset \mathcal{U}$ .

Moreover, let the system  $(A, B, \tilde{\mathcal{U}})$  be normal. If  $u$  is an optimal control for the OCP with the input constraint  $u \in \tilde{\mathcal{U}}$ . Then, it is an optimal control for the original OCP and  $u(t) \in \text{ex}(\mathcal{U})$  for almost every  $t \in [0, t_f]$ .

Thus, normality emerges as the key property enabling lossless convexification of the OCP. This result was presented for OCPs in Mayer-form but can be extended to Lagrange-form using an epigraph as suggested in [6]. However, no results are presented on whether using an epigraph transformation preserves the normality of the system, a property which is needed in order to ensure the lossless convexification of the problem.

#### IV. EQUIVALENT FORMULATION IN MAYER-FORM

To write problem 1 as a Mayer-form OCP, we use an epigraph transformation [15], which also provides a continuous relaxation of the cost function (3a). Define the maximum and minimum of the running cost function (3a) over the set  $\mathcal{U}$

$$\bar{u} \triangleq \max_{u \in \mathcal{U}} \|u\|_1, \quad u \triangleq \min_{u \in \mathcal{U}} \|u\|_1 = 0.$$

Then, let  $\nu(t) \in [\underline{u}, \bar{u}]$  be a slack input and define the augmented input set

$$\mathcal{U}_e \triangleq \{(u, \nu) : u \in \mathcal{U}, \|u(t)\|_1 \leq \nu(t) \leq \bar{u}\}.$$

Next, let  $x_c(t) \in \mathbb{R}$  be the cost state variable which satisfies the dynamics

$$\dot{x}_c(t) = \nu(t), \quad (6)$$

with the initial condition  $x_c(0) \triangleq 0$ . Then, consider the augmented state  $x_e \triangleq [x^\top \quad x_c]^\top$  and input  $u_e \triangleq [u \quad \nu]$ . The augmented system is

$$\dot{x}_e(t) = A_e x_e(t) + B_e u_e(t), \quad (7)$$

where

$$A_e \triangleq \begin{bmatrix} A & 0 \\ 0 & 0 \end{bmatrix}, \quad B_e \triangleq \begin{bmatrix} B & 0 \\ 0 & 1 \end{bmatrix}.$$

Then, consider the OCP in Mayer-form.

#### Problem 2. Mayer-form Mixed-Integer Problem

$$\min_{u_e(t)} x_c(t_f) \quad (8a)$$

$$\text{subject to } \dot{x}_e(t) = A_e x_e(t) + B_e u_e(t), \quad (8b)$$

$$u_c \in \mathcal{U}_e, \quad (8c)$$

$$x(0) = x_0, \quad x(t_f) = 0, \quad (8d)$$

$$x_c(0) = 0 \quad (8e)$$

The following result shows that Problem 1 and Problem 2 are equivalent.

**Lemma 4.** Consider Problem 1 and its Mayer-form reformulation Problem 2. Any optimal control  $u^*$  of Problem 2 is also an optimal control of Problem 1.

*Proof.* Consider the Hamiltonian (4). The costate dynamics are given by

$$\dot{p}(t) = -\frac{\partial H_1}{\partial x} = -A^\top p(t),$$

and the minimization condition (5) implies that for almost every  $t \in [0, t_f]$

$$u^*(t) \in \arg \min_{u \in \mathcal{U}} \{ \|u(t)\|_1 + (B^\top p(t))^\top u(t) \}. \quad (9)$$

To write the Hamiltonian for Problem 2, we first find an equivalent running cost for (8a). Note that the solution to (6) is

$$x_c(t_f) = \int_0^{t_f} \nu(t) dt. \quad (10)$$

Therefore, the terminal cost (8a) is equivalent to the running cost (10). Then, consider the Hamiltonian for Problem 2, where  $p_c(t) \in \mathbb{R}$  is the costate variable for the auxiliary cost state with  $p_c(t_f) = 1$  due to the transversality condition

$$H_2(x, u, p = \nu + p^\top (Ax + Bu) + p_c \nu.$$

The costate dynamics are given by

$$\dot{p}(t) = -\frac{\partial H_2}{\partial x} = -A^\top p(t), \quad \dot{p}_c(t) = -\frac{\partial H_2}{\partial x_c} = 0.$$

Since  $\dot{p}_c(t) = 0$  and  $p_c(t_f) = 1$ , then the minimization condition (5) implies that for almost every  $t \in [0, t_f]$

$$u_e^*(t) \in \arg \min_{u_e \in \mathcal{U}_e} \{ (B^\top p(t))^\top u(t) + 2\nu(t) \}.$$

Note that  $u$  and  $\nu$  are uncoupled in the Hamiltonian of Problem 2, which implies that they can be minimized separately. To minimize the slack input,  $2\nu(t)$  must be minimized subject to the constraint  $\|u(t)\|_1 \leq \nu(t)$ . Since the term  $2\nu(t)$  is affine then the minima is found when the constraint is active, which implies

$$\nu^*(t) = \|u^*(t)\|_1 \quad (11)$$

Next, substituting (11) into the minimization condition of Problem 2 yields

$$u^*(t) \in \arg \min_{u \in \mathcal{U}} \{ 2\|u(t)\|_1 + (B^\top p(t))^\top u(t) \}. \quad (12)$$

Since  $\|u\|_1 \geq 0$  for all  $u$  and the associated costate dynamics are the same for Problem 1 and Problem 2, minimizing (9) and (12) over the finite set  $\mathcal{U}$  results in the same optimal control. Therefore, the optimal control of Problem 2 is the optimal control of Problem 1.  $\square$

As shown in Lemma 4, the original Lagrange-form OCP has been reformulated as a Mayer-form OCP. In the next section, we proceed with the lossless convexification of this Mayer-form problem.

## V. NORMALITY FOR LOSSLESS CONVEXIFICATION

Consider the convex relaxation of the input set

$$\tilde{\mathcal{U}} \triangleq \text{conv}(\mathcal{U}). \quad (13)$$

**Fact 2.** Consider the input set  $\mathcal{U}$  and the convex relaxation  $\tilde{\mathcal{U}}$ . The following holds:

- 1)  $\mathcal{U} \subset \tilde{\mathcal{U}}$ .
- 2)  $\text{ex}(\tilde{\mathcal{U}}) \subset \mathcal{U}$ .
- 3)  $\tilde{\mathcal{U}}$  is a compact convex polytope.

*Proof.* The first claim follows directly from the definition of the convex hull.

To prove the second claim, since  $\mathcal{U}$  is finite,  $\tilde{\mathcal{U}}$  is a convex polytope. By definition, the extreme points of a convex polytope are always a subset of the points used to generate it. Thus,  $\text{ex}(\tilde{\mathcal{U}}) \subset \mathcal{U}$ .

The third claim follows directly from fact 1.  $\square$

Next, we define the relaxed augmented input set

$$\tilde{\mathcal{U}}_e \triangleq \{(u, \nu) : u \in \tilde{\mathcal{U}}, \|u(t)\|_1 \leq \nu(t) \leq \bar{u}\}.$$

The following result plays a critical role in establishing the normality of the augmented system.

**Fact 3.** Consider the sets  $\mathcal{U}$ ,  $\mathcal{U}_e$  and the convex relaxations  $\tilde{\mathcal{U}}$  and  $\tilde{\mathcal{U}}_e$ . Then, the following holds:

- 1)  $\mathcal{U}_e \subset \tilde{\mathcal{U}}_e$ .
- 2)  $\text{ex}(\tilde{\mathcal{U}}_e) \subset \mathcal{U}_e$ .
- 3)  $\tilde{\mathcal{U}}_e$  is a compact convex polytope.

*Proof.* To prove the first claim, note from fact 2 that  $\mathcal{U} \subset \tilde{\mathcal{U}}$ . Since every  $(u, \nu) \in \mathcal{U}_e$  satisfies  $u \in \mathcal{U}$  and  $\|u\|_1 \leq \nu \leq \bar{u}$ , it follows that  $(u, \nu) \in \tilde{\mathcal{U}}_e$ . Hence,  $\mathcal{U}_e \subset \tilde{\mathcal{U}}_e$ .

For the second claim, consider the extreme points of  $\tilde{\mathcal{U}}_e$ . By definition,  $\tilde{\mathcal{U}}_e$  is the intersection of the convex polytope  $\tilde{\mathcal{U}} \times [\underline{u}, \bar{u}]$  with the epigraph constraint  $\nu \geq \|u\|_1$ . Therefore, extreme points of  $\tilde{\mathcal{U}}_e$  must lie either on the lower boundary  $\nu = \|u\|_1$  or on the upper boundary  $\nu = \bar{u}$ . It follows from fact 1 that since  $\tilde{\mathcal{U}} = \mathcal{C}_m(u_{\max})$ , then (A1) is satisfied. By Assumption (A1), whenever  $u$  is an extreme point of  $\tilde{\mathcal{U}}$ , the corresponding  $\nu$ -coordinate satisfies  $\nu = \|u\|_1$  or  $\nu = \bar{u}$ , and in both cases  $(u, \nu) \in \mathcal{U}_e$ . Thus,  $\text{ex}(\tilde{\mathcal{U}}_e) \subset \mathcal{U}_e$ .

To prove the third claim, note from fact 2 that  $\tilde{\mathcal{U}}$  is a compact convex polytope. The epigraph of the  $\ell_1$ -norm,  $\{(u, \nu) : \nu \geq \|u\|_1\}$ , is a polyhedral set since  $\|u\|_1 = \max_{s \in \{\pm 1\}^m} s^\top u$ . Hence,  $\tilde{\mathcal{U}}_e = (\tilde{\mathcal{U}} \times [\underline{u}, \bar{u}]) \cap \{(u, \nu) : \nu \geq \|u\|_1\}$  is the intersection of a bounded polyhedron and a polyhedral set, and is therefore a compact convex polytope.  $\square$

Now we can explain the technical importance of (A1). As seen in fact 3, this assumption ensures that the extreme points of the set  $\tilde{\mathcal{U}}_e$  are contained in  $\mathcal{U}_e$ , which in turn guarantees that  $\tilde{\mathcal{U}}_e$  is compact. If (A1) is not imposed, then  $\tilde{\mathcal{U}}_e$  could be

closed but unbounded, as vertical edges in  $\tilde{\mathcal{U}}$  would allow  $\nu$  to increase without bound while keeping  $u$  fixed. This would violate compactness and undermine the convex relaxation framework.

Figure 2 illustrates the sequence of relaxations used to convexify the discrete input set  $\mathcal{U}$ . The convex relaxation  $\tilde{\mathcal{U}}$  takes the form of a cross-polytope in  $\mathbb{R}^2$ , consistent with fact 1. By applying the epigraph transformation, we obtain the augmented set  $\tilde{\mathcal{U}}_e$ , whose convex relaxation  $\tilde{\mathcal{U}}_e$  is a compact convex polytope as established in fact 3.

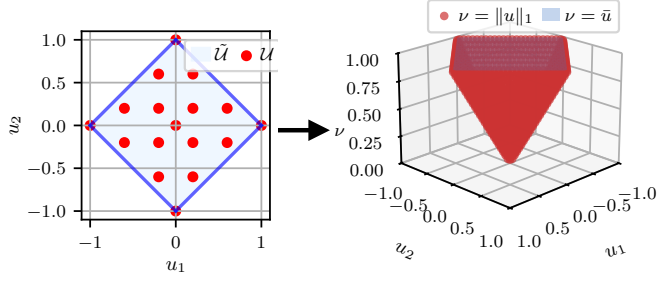


Fig. 2. Discrete input set  $\mathcal{U}$  and its convex relaxation  $\tilde{\mathcal{U}}$  which forms a cross-polytope. The epigraph-based augmented set  $\tilde{\mathcal{U}}_e$  yields a compact convex polytope.

The following lemma establishes the normality of the augmented system  $(A_e, B_e, \tilde{\mathcal{U}}_e)$ , by analyzing the normality of the original system alone.

**Lemma 5.** Consider (2) and the input set  $\mathcal{U}$ . Assume (A2) holds. Then, the augmented system  $(A_e, B_e, \tilde{\mathcal{U}}_e)$  is normal.

*Proof.* Since  $(A, B)$  is controllable, it follows that  $(A_e, B_e)$  is controllable, and by definition  $\tilde{\mathcal{U}}_e = \text{conv}(\mathcal{U}_e)$ . Then, it follows from lemma 1 that  $(A_e, B_e)$  is normal with respect to  $\tilde{\mathcal{U}}_e$ .  $\square$

Lemma 5 implies that normality is preserved under the reformulations employed in this work to reach the OCP in Mayer-form. Next, consider the convex relaxation of Problem 2

### Problem 3. Smooth Mayer-form Fuel-Optimal Problem

$$\min_{u_e(t)} x_c(t_f) \quad (14a)$$

$$\text{subject to } \dot{x}_e(t) = A_e x_e(t) + B_e u_e(t), \quad (14b)$$

$$u_e \in \tilde{\mathcal{U}}_e, \quad (14c)$$

$$x(0) = x_0, \quad x(t_f) = x_f, \quad (14d)$$

$$x_c(0) = 0 \quad (14e)$$

The following theorem presents the main result.

**Theorem 1.** Consider Problem 1 and Problem 3. Assume (A2) holds. If  $(u^*, \nu^*)$  is an optimal control of Problem 3, then  $u^*$  is an optimal control of Problem 1.

*Proof.* By lemma 5, the augmented system  $(A_e, B_e, \tilde{\mathcal{U}}_e)$  is normal. From fact 3, the set  $\tilde{\mathcal{U}}_e$  satisfies conditions (C1)–(C3), allowing the use of extreme-point relaxation.

Then, lemma 3 implies that the optimal control  $(u^*, \nu^*)$  of Problem 3 is also an optimal control for Problem 2, and moreover  $u^*(t) \in \text{ex}(\tilde{\mathcal{U}}) \subseteq \mathcal{U}$  a.e.  $t \in [0, t_f]$ .

Finally, applying lemma 4, the optimal control of Problem 2 is also an optimal control of Problem 1. Therefore,  $u^* \in \mathcal{U}$  is an optimal control of Problem 1.  $\square$

Theorem 1 confirms that the lossless convexification exactly recovers a solution of the original discrete-valued optimal control problem by solving the relaxed convex problem. This theorem provides a systematic way to establish the lossless convexification of the fuel-optimal control problem with discrete-valued inputs. Fig. 3 illustrates the logical flow of the equivalent reformulations of the OCP.

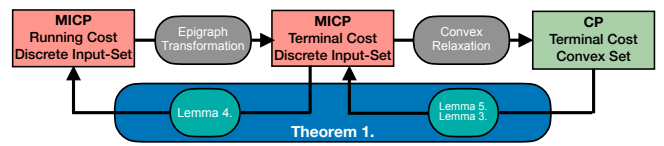


Fig. 3. The discrete-input OCP (MICP) with running costs is transformed via the epigraph formulation and convex relaxation steps, leading to the final equivalence stated in theorem 1.

Importantly, the scope of this result extends beyond the fuel-optimal problem. In particular, the same convexification approach also applies to the maximum-hands-off control problem, a widely studied nonconvex OCP where the running cost is measured using the  $L^0$ -norm of the control input. This is formalized in the following corollary.

**Corollary 1.** The lossless convexification established in Theorem 1 also applies to the maximum-hands-off control problem, whose running cost is given by  $\phi(u) = \int_0^{t_f} \|u(t)\|_0 dt$ .

*Proof.* This follows directly from [11, Theorem 8], which shows that the fuel-optimal control problem serves as a convex relaxation of the maximum-hands-off problem. Therefore, by Theorem 1, the lossless convexification also yields the exact solution to the maximum-hands-off problem.  $\square$

## VI. NUMERICAL SIMULATIONS

We illustrate the effectiveness of the lossless convexification framework through a low-Earth orbit satellite rendezvous problem. Consider a non-cooperative chief spacecraft orbiting in a near-circular orbit, and consider a chaser spacecraft with cold-gas thruster actuators in its three orthogonal directions. The relative motion of the chaser spacecraft with respect to the chief spacecraft is modeled using the Clohessy–Wiltshire (CW) equations [16].

Let  $x(t) \triangleq [r(t)^\top \quad v(t)^\top]^\top$  be the state vector consisting of the relative position and velocity, and let  $u \in \mathcal{U} \subset \mathbb{R}^3$  be

the control input. The system matrices for (2) are given by

$$A \triangleq \begin{bmatrix} 0 & 0 & 0 & 1 & 0 & 0 \\ 0 & 0 & 0 & 0 & 1 & 0 \\ 0 & 0 & 0 & 0 & 0 & 1 \\ 3n^2 & 0 & 0 & 0 & 2n & 0 \\ 0 & 0 & 0 & -2n & 0 & 0 \\ 0 & 0 & -n^2 & 0 & 0 & 0 \end{bmatrix}, B \triangleq \begin{bmatrix} 0 & 0 & 0 \\ 0 & 0 & 0 \\ 0 & 0 & 0 \\ 1 & 0 & 0 \\ 0 & 1 & 0 \\ 0 & 0 & 1 \end{bmatrix},$$

where  $n = \sqrt{\frac{\mu}{R^3}}$  is the mean motion of the chief spacecraft,  $\mu$  is the standard gravitational parameter, and  $R = 7102.8 \cdot 10^3$  m is the radius of the chief spacecraft's circular orbit. Note that  $(A, B)$  is controllable, hence (A2) is satisfied.

The actuators are limited by a maximum acceleration  $u_{\max} > 0$ . The admissible input set  $\mathcal{U}$  includes all combinations in which the actuators share this magnitude in a structured way, a common constraint in small satellites[10]:

- A single actuator operates at full magnitude, while the others are off:  $\pm u_{\max} e_i$ ,  $i = 1, 2, 3$ .
- Two actuators share the input equally:  $\pm \frac{u_{\max}}{2} (e_i + e_j)$ ,  $i, j = 1, 2, 3$ ,  $i \neq j$ .
- All three actuators are active with equal contribution:  $\pm \frac{u_{\max}}{3} (1, 1, 1)$ .

Here,  $e_i$  denotes the  $i$ -th standard basis vector in  $\mathbb{R}^3$ . Note that this input set follows the structure from (1). Thus, it follows from fact 1 that (A1) holds, enabling the use of lossless convexification to solve the fuel-optimal control problem from theorem 1.

While theorem 1 is established in continuous time, numerical solvers work with finite-dimensional parameters. To solve Problem 3, we discretize the time horizon into a grid of  $N > 0$  sample points, and apply a zero-order hold to discretize the dynamics (14b). This reformulation yields a finite-dimensional problem, which we solve using CVXPY [17] with the ECOS solver on a MacBook Air equipped with an Apple M1 chip and 16 GB of RAM.<sup>1</sup>

The output of the numerical optimization is a control sequence  $\{u_k\}_{k=0}^N$ . To evaluate the quality of the solutions, we introduce the following metrics: distance of a control input  $u_k$  to the discrete set and the average distance of the control sequence to the discrete set, which are defined as

$$d(u_k) \triangleq \min_{\zeta \in \mathcal{U}} \|u_k - \zeta\|_2, \quad \bar{d}(u) \triangleq \frac{1}{N} \sum_{k=0}^N d(u_k),$$

respectively. These metrics characterize the discreteness of the solution, at the level of individual control inputs as well as the entire control sequence.

#### A. Validation of Lossless Convexification

We first demonstrate that the resulting optimal control from Problem 3 is discrete-valued, thereby verifying that the relaxation is lossless. A dense discretization grid is employed to closely approximate the continuous-time solution. For real-time applications, coarser grids may be adopted to reduce computational effort, as discussed in section VI-B.

<sup>1</sup>The implementation is available at: [https://github.com/FelipeArenasUribe/MICP\\_LosslessConvexification](https://github.com/FelipeArenasUribe/MICP_LosslessConvexification)

Consider the initial conditions  $r_0 = [-100 \ -500 \ -100]$  m and  $v_0 = [0 \ 0 \ 0]$  m/s, with a final time of  $t_f = 240$  s. The problem is discretized using  $N = 800$  grid points, and the optimization is solved in 0.252 seconds. Fig. 4 shows the system states throughout the trajectory, converging to the desired terminal conditions at  $t_f$ .

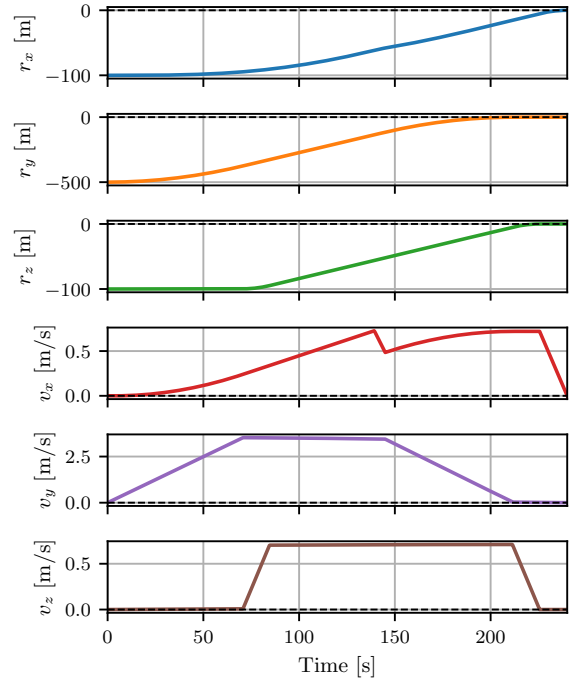


Fig. 4. System states during rendezvous, showing convergence to the desired terminal conditions.

The corresponding optimal control inputs are shown in Fig. 5. The dashed lines denote the admissible control values in the discrete set  $\mathcal{U}$ . For almost every  $t \in [0, t_f]$ , the optimal control  $u(t) \in \mathcal{U}$ . The average distance to the discrete set is  $\bar{d}(u) = 0.00622$  m/s<sup>2</sup>, indicating that the control sequence is effectively discrete-valued.

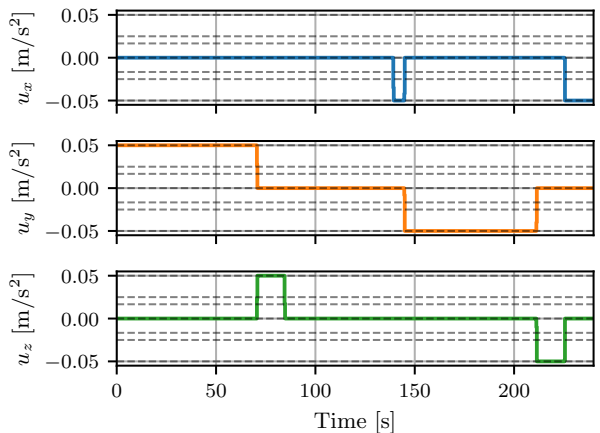


Fig. 5. Optimal control inputs with respect to the admissible discrete set  $\mathcal{U}$ . The dashed lines represent the admissible inputs.

## B. Maintaining Discrete-Valued Controls with Reduced Grid Resolution

Although the previous case already demonstrates efficient performance, further improvements can be achieved by reducing the number of grid points (i.e., decision variables). Since the complexity of convex optimization problems scales polynomially with the number of decision variables [15], we can obtain improved performance in solver time by reducing the number of grid points.

To demonstrate that the discreteness of the solution is preserved even when reducing the number of grid points, we perform the following experiment. For a fixed final time  $t_f = 300$  s, we randomly sample 10 initial conditions from the set  $\mathcal{X}_0 \triangleq \{x \in \mathbb{R}^6 : \|r\|_\infty \leq 500, \|v\|_\infty \leq 5\}$  using an uniform distribution. For each initial condition, Problem 3 is solved with different numbers of grid points  $N$ , increasing from  $N_0 = 100$  to  $N_f = 1000$  in steps of 100.

Fig. 6 shows the mean solver time and the average distance of the trajectories to the discrete control set. As expected, solver time increases approximately linearly with the number of grid points, while the average distance decreases, indicating improved adherence to the discrete set. The remaining quantization error is small and can be readily compensated through feedback control. Notably, beyond  $N = 400$ , the metric decreases only marginally, suggesting that further increasing the grid size yields limited gains in control discreteness.

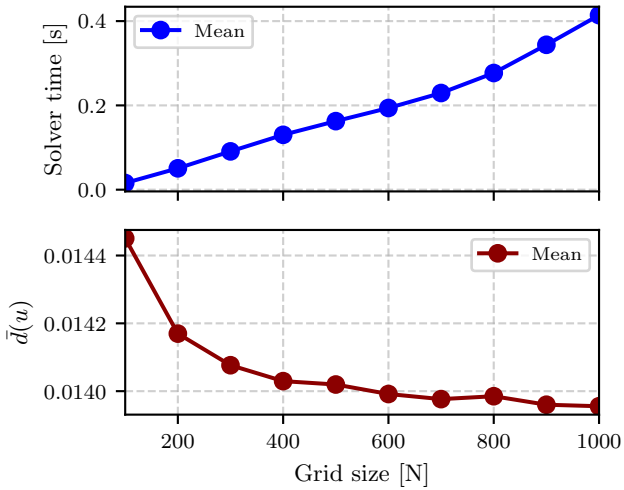


Fig. 6. Effect of grid size on solver time and control discreteness. Increasing the number of grid points improves adherence to the discrete control set but increases computational time.

## C. Real-time Performance

Real-time spacecraft control guidelines from NASA's Safe & Precise Landing Integrated Capabilities Evolution (SPLICE) project specify a guidance update-rate requirement of 3 seconds, with a target goal of 1 second [12]. These values apply to both attitude and position guidance, which constitutes a considerably more challenging problem and remains a direction for future work. Nevertheless, they provide a useful benchmark for evaluating the performance of our algorithm.

To evaluate the consistent performance of the algorithm in producing discrete-valued controls for real-time applications, we perform a Monte Carlo simulation. A total of 1000 initial conditions are randomly sampled from  $\mathcal{X}_0$  using an uniform distribution. For each initial condition, the optimization problem is solved for a fixed final time  $t_f = 300$  s using a grid with  $N = 400$  sample points.

The Monte Carlo simulation demonstrates that the solver time for all 1000 sampled initial conditions is below 1 s (see Fig. 7), satisfying the SPLICE guidance update-rate goal. The mean and median solver times are 0.107 s and 0.083 s, respectively, indicating some variability across initial conditions. Overall, these results confirm that the algorithm is capable of providing real-time feasible control solutions.

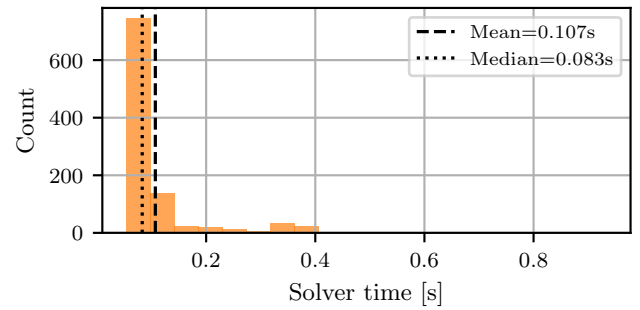


Fig. 7. Histogram of solver times from the Monte Carlo simulation. All solver times are below 1 s, demonstrating real-time feasibility for the selected grid.

The average distance to the discrete control set  $\bar{d}(u)$  across the Monte Carlo simulations is shown in Fig. 8. The distribution of  $\bar{d}(u)$  is approximately normal, the mean value of 0.012 m/s<sup>2</sup> indicates that the algorithm consistently produces discrete-valued controls, validating that the relaxation is effectively lossless for all tested initial conditions.

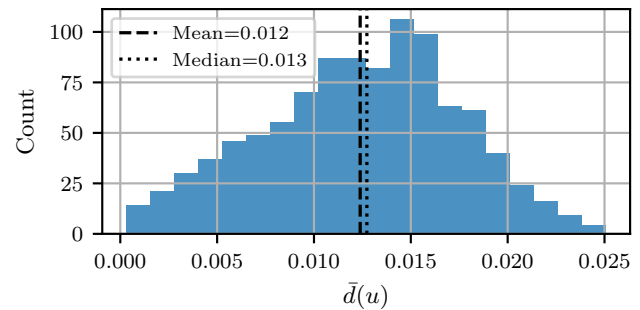


Fig. 8. Histogram of the average distance to the discrete set  $\bar{d}(u)$  from the Monte Carlo simulation. The small mean value demonstrates that the algorithm reliably produces discrete-valued controls.

## VII. CONCLUSIONS

This paper presented a method to solve the fuel-optimal control problem for linear systems with finite, disconnected control input sets. By leveraging lossless convexification, the mixed-integer convex program is transformed into an equivalent convex program under normality conditions, enabling efficient and reliable real-time implementation. We

extended existing normality results by providing simple geometric criteria for linear systems with cross-polytopic input sets and showed that normality is preserved when reformulating Lagrange-form optimal control problems into Mayer-form. Numerical simulations demonstrate that the algorithm consistently produces discrete-valued controls while meeting real-time computational requirements, with solver times well below one second. These results confirm the practical feasibility of the proposed framework for real-time spacecraft guidance applications. Future work includes incorporating state constraints while preserving input discreteness, as well as extending the approach to Model Predictive Control frameworks.

## REFERENCES

- [1] T. Achterberg, R. Wunderling, Mixed Integer Programming: Analyzing 12 Years of Progress, Springer Berlin Heidelberg, Berlin, Heidelberg, 2013. doi:10.1007/978-3-642-38189-8\_18.
- [2] D. Malyuta, Y. Yu, P. Elango, B. Açıkmese, Advances in trajectory optimization for space vehicle control, *Annual Reviews in Control* 52 (2021) 282–315. doi:<https://doi.org/10.1016/j.arcontrol.2021.04.013>.
- [3] A. Cauligi, P. Culbertson, E. Schmerling, M. Schwager, B. Stellato, M. Pavone, Coco: Online mixed-integer control via supervised learning, *IEEE Robotics and Automation Letters* 7 (2) (2022) 1447–1454. doi:10.1109/LRA.2021.3135931.
- [4] A. Cauligi, P. Culbertson, B. Stellato, D. Bertsimas, M. Schwager, M. Pavone, Learning mixed-integer convex optimization strategies for robot planning and control, in: 2020 59th IEEE Conference on Decision and Control (CDC), 2020, pp. 1698–1705. doi:10.1109/CDC42340.2020.9304043.
- [5] D. Malyuta, T. P. Reynolds, M. Szmułk, T. Lew, R. Bonalli, M. Pavone, B. Açıkmese, Convex optimization for trajectory generation: A tutorial on generating dynamically feasible trajectories reliably and efficiently, *IEEE Control Systems Magazine* 42 (5) (2022) 40–113. doi:10.1109/MCS.2022.3187542.
- [6] M. W. Harris, Optimal control on disconnected sets using extreme point relaxations and normality approximations, *IEEE Transactions on Automatic Control* (2021) 1–1 doi:10.1109/tac.2021.3059682.
- [7] N. T. Woodford, M. W. Harris, Geometric properties of time-optimal controls with state constraints using strong observability, *IEEE Transactions on Automatic Control* 67 (12) (2022) 6881–6887. doi:10.1109/TAC.2021.3134627.
- [8] I. M. Ross, How to find minimum-fuel controllers, aIAA Paper No. 2004-5346, Session: GNC-43: Spacecraft Control and Applications (2004). doi:10.2514/6.2004-5346.
- [9] I. M. Ross, Space Trajectory Optimization and L1-Optimal Control Problems, Vol. 1 of Elsevier Astrodynamics Series, Butterworth-Heinemann, 2006.
- [10] S. V. Weston, C. D. Burkhard, J. M. Stupl, R. L. Ticknor, B. D. Yost, R. A. Austin, P. Galchenko, L. K. Newman, L. S. Soto, State-of-the-art small spacecraft technology, NASA Technical Publication NASA/TP-20250000142, National Aeronautics and Space Administration (NASA), Ames Research Center, Moffett Field, CA (February 2025).
- [11] M. Nagahara, D. E. Quevedo, D. Nešić, Maximum hands-off control: A paradigm of control effort minimization, *IEEE Transactions on Automatic Control* 61 (3) (2016) 735–747. doi:10.1109/TAC.2015.2452831.
- [12] J. A. Doll, A. G. Kamath, K. W. Smith, J. M. Harper, I. Rowe, B. Açıkmese, S. M. Pedrotty, G. F. Mendeck, Hardware in the Loop Performance of Terrestrial Powered Descent Dual Quaternion Guidance With a Custom First-Order Solver, in: AIAA SCITECH 2025 Forum, American Institute of Aeronautics and Astronautics, Orlando, FL, 2025. doi:10.2514/6.2025-2776.
- [13] L. D. Berkovitz, N. G. Medhin, Nonlinear Optimal Control Theory, 1st Edition, Chapman and Hall/CRC, 2012. doi:10.1201/b12739.
- [14] R. T. Rockafellar, Convex Analysis, Princeton University Press, Princeton, 1970. doi:doi:10.1515/9781400873173.
- [15] S. Boyd, L. Vandenberghe, Convex optimization, Cambridge University Press, 2004.
- [16] H. Curtis, Orbital Mechanics: For Engineering Students, Aerospace Engineering, Butterworth-Heinemann, 2015.
- [17] S. Diamond, S. Boyd, CVXPY: A Python-embedded modeling language for convex optimization, *Journal of Machine Learning Research* 17 (83) (2016) 1–5.